A DFT Study of the Interresidue Dependencies of Scalar *J*-Coupling and Magnetic Shielding in the Hydrogen-Bonding Regions of a DNA Triplex

Michael Barfield,*,† Andrew J. Dingley,‡ Juli Feigon,§ and Stephan Grzesiek*,||

Contribution from the Department of Chemistry, University of Arizona, Tucson, Arizona 85721, Institute of Physical Biology, Heinrich-Heine-Universität, 40225 Düsseldorf, Germany, Department of Chemistry and Biochemistry, University of California, Los Angeles, California 90095, and Department of Structural Biology, Biozentrum, University of Basel, CH-4056 Basel, Switzerland

Received October 25, 2000. Revised Manuscript Received January 23, 2001

Abstract: Scalar coupling constants and magnetic shieldings in the imino hydrogen-bonding region of Hoogsteen−Watson−Crick T·A-T and C^+·G−C triplets have been calculated as a function of the distance between proton donor and acceptor nitrogen atoms. The Fermi contact contributions to $^{h2}J(^{15}N-H\cdots{}^{15}N)$, $^{1}J(^{15}N-^{1}H)$, and $^{h1}J(^{1}H\cdots{}^{15}N)$ were computed using density functional theory/finite perturbation theory (DFT/FPT) methods for the full base triplets at the unrestricted B3PW91/6-311G** level. Chemical shifts $\delta(^{1}H)$ and $\delta(^{15}N)$ were obtained at the same level using the gauge including atomic orbital (GIAO) method for magnetic shielding. All three scalar couplings and all three chemical shifts are strongly interrelated and exhibit monotonic changes with base pair separation. These correlations are in conformity with experimental data for a 32-nucleotide DNA triplex. The results suggest that both chemical shifts and coupling constants can be used to gain information on H-bond donor−acceptor distances in nucleic acids. In addition to the DFT/FPT calculations, a simple three-orbital model of the N−H···H bond and a sum-over-states analysis is presented. This model reproduces the basic features of the H-bond coupling effect. In accordance with this model and the DFT calculations, a positive sign for the $^{h2}J_{NN}$ coupling is determined from an E.COSY experiment.

Introduction

The use of interresidue coupling constants as an unequivocal indication of hydrogen-bonding interactions[1−8] complements other more indirect parameters[9] such as quadrupolar broadening,[10] isotope effects,[11] and isotropic chemical shifts[12−17] for resonance assignments and conformational analyses in DNA, RNA, and proteins. Since coupling constants are very sensitive to the electronic features of hydrogen bonds,[18,19] a detailed analysis offers the potential to extract important structural information. A number of recent computational studies[3,20−24] using density functional theory and ab initio MO methods have reproduced the size and trends of the observed coupling constants in the imino group H-bonds of Watson−Crick base

* To whom correspondence should be sent. M.B.: (phone) +1 520 621 6348; (fax) +1 520 621 8407; (e-mail) Barfield@u.arizona.edu. S.G.: (phone) ++41 61 267 2100; (fax) ++41 61 267 2109; (e-mail) Stephan.Grzesiek@unibas.ch.

† University of Arizona.

‡ Heinrich-Heine-Universität.

§ University of California, Los Angeles.

|| University of Basel.

(1) Dingley, A. J.; Grzesiek, S. *J. Am. Chem. Soc*. **1998**, *120*, 8293−8297.

(2) Pervushin, K.; Ono, A.; Fernández, C.; Szyperski, T.; Kainosho, M.; Wüthrich, K. *Proc. Natl. Acad. Sci, U.S.A.* **1998**, *95*, 14147−14151.

(3) Dingley, A. J.; Masse, J. E.; Peterson, R. D.; Barfield, M.; Feigon, J.; Grzesiek, S. *J. Am. Chem. Soc*. **1999**, *121*, 6019−6027.

(4) Cornilescu, G.; Hu, J.-S.; Bax, A. *J. Am. Chem. Soc.* **1999**, *121*, 2949−2950.

(5) Cordier, F.; Grzesiek, S. *J. Am. Chem. Soc*. **1999**, *121*, 1601−1602.

(6) Pervushin, K.; Fernández, C.; Riek, R.; Ono, A.; Kainosho, M.; Wüthrich, K. *J. Biomol. NMR* **2000**, *16*, 39−46.

(7) Majumdar, A.; Kettani, A.; Skripkin, E. *J. Biomol. NMR* **1999**, *14*, 67−70.

(8) Kettani, A.; Gorin, A.; Majumdar, A.; Hermann, T.; Skripkin, E.; Zhao, H.; Jones, R.; Patel, D. J. *J. Mol. Biol.* **2000**, *297*, 627−644.

(9) Becker, E. D. In *Encyclopedia of Nuclear Magnetic Resonance*; Grant, D. M., Harris, R. K., Eds., Wiley: New York, 1996; pp 2400−2415.

(10) Koole, L. H.; De Boer, H.; De Haan, J. W.; Haasnoot, C. A. G.; Van Dael, P.; Buck, H. M. *J. Chem. Soc., Chem. Commun*. **1986**, 362−364.

(11) Wang, C.; Gao, X.; Jones, R. A. *J. Am. Chem. Soc*. **1991**, *113*, 1448−1450.

(12) Kearns, D. R.; Shulman, R. G. *Nature* **1971**, *229*, 338−339. Kearns, D. R.; Patel, D. J.; Shulman, R. G.; Yamane, T. *J. Mol. Biol*. **1971**, *61*, 265−270.

(13) Kearns, D. R.; Lightfoot, D. R.; Wong, K. L.; Wong, Y. P.; Reid, B. R.; Cary, L.; Shulman, R. G. *Ann. N. Y. Acad. Sci*. **1973**, *222*, 324−336.

(14) Poulter, C. D.; Livingston, C. L. *Tetrahedron Lett*. **1979**, 755−758.

(15) Griffey, R. H.; Redfield, A. G. *Q. Rev. Biophys*. **1987**, *19*, 51−82 and references therein.

(16) Moore, P. B. *Acc. Chem. Res*. **1995**, *28*, 251−256.

(17) Zhang, X.; Gaffney, B. L.; Jones, R. A. *J. Am. Chem. Soc*. **1998**, *120*, 6625−6626.

(18) Shenderovich, I. G.; Smirnov, S. N.; Denisov, G. S.; Gindin, V. A.; Golubev, N. S.; Dunger, A.; Reibke, R.; Kirpekar, S.; Malkina, O. L.; Limbach, H.-H. *Ber. Bunsen-Ges. Phys. Chem.* **1998**, *102*, 422−428.

(19) Golubev, N. S.; Shenderovich, I. G.; Smirnov, S. N.; Denisov, G. S.; Limbach, H.-H. *Chem. Eur. J*. **1999**, *5*, 492−497.

(20) Benedict, H.; Shenderovich, I. G.; Malkina, O. L.; Malkin, V. G. Denisov, G. S.; Golubev, N. S.; Limbach, H.-H. *J. Am. Chem. Soc.* **2000**, *122*, 1979−1988.

(21) Scheurer, C.; Brüschweiler, R. *J. Am. Chem. Soc*. **1999**, *121*, 8661−8662.

(22) Perera, S. A.; Bartlett, R. J. *J. Am. Chem. Soc*. **2000**, *122*, 1231−1232. Del Bene, J. E.; Perera, S. A.; Bartlett, R. J. *J. Am. Chem. Soc*. **2000**, *122*, 3560−3561.

(23) Pecul, M.; Leszczynski, J.; Sadlej, J. *J. Chem. Phys*. **2000**, *112*, 7930−7938. Pecul, M.; Leszczynski, J.; Sadlej, J. *J. Phys. Chem.* **2000**, *104*, 8105−8113.

(24) Galasso, V. *Int. J. Quantum Chem*. **1998,** *70*, 313−320.

10.1021/ja003781c CCC: $20.00
Published on Web 04/25/2001

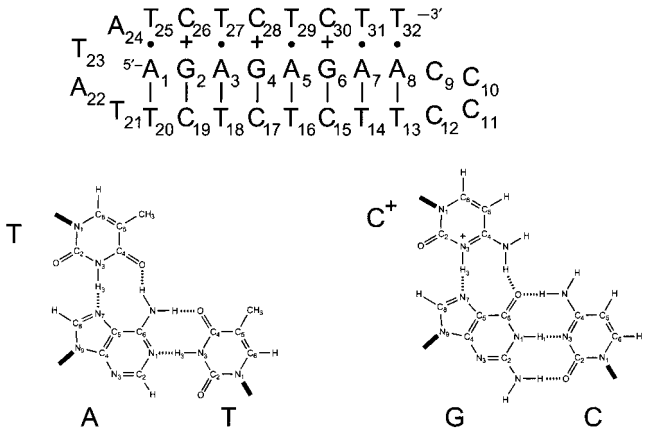

Figure 1. (Top) Sequence and base-pairing scheme of the 32-nucleotide intramolecular DNA triplex used in this study. (Bottom) Chemical formulas and numbering schemes for the C$^+$·G−C and T·A−T triplets.

pairs and in the amide-to-carbonyl H-bonds in proteins, as well as in smaller molecules.[24]

A number of computational studies on the chemical shifts associated with base pairs in DNA and RNA have appeared.[25−30] However, unified computational analyses of both coupling constants and chemical shifts of donor and acceptor groups as a function of the hydrogen bond geometry have not, heretofore, been carried out for the full base pairs. This study extends the current theoretical description of H-bond couplings in two ways: (1) the observed trends in the $^{h2}J_{NN}$, $^{h1}J_{NH}$, and $^{1}J_{NH}$ coupling constants[31] are reproduced by adopting a simple three-orbital MO model for the N−H···N hydrogen bond; (2) a combined approach uses density functional theory (DFT) methods (finite perturbation theory (FPT) and gauge including atomic orbitals) to calculate the three H-bond coupling constants and three chemical shifts of the nuclei in the N−H···N hydrogen bond. Computations are performed for the full Hoogsteen−Watson−Crick C$^+$·G−C and T·A−T triplets (depicted in Figure 1) as a function of the H-bond lengths. The DFT results compare favorably with experimental data observed in a recent study of the intramolecular 32-nucleotide DNA triplex depicted in Figure 1.

Computational Methods

Molecular Structures. Ab initio and DFT studies of base pair structures have demonstrated that the inclusion of electron correlation is important for adequate descriptions of hydrogen bonding and NH_2 group orientations.[32] Here, all molecular geometries are fully optimized using the Gaussian 94 codes[33,34] with split valence basis sets and polarization functions at the B3PW91/6-31G** level of density functional theory.[35,36] Polarization functions on hydrogen atoms were included in the geometry optimizations because of their importance in describing hydrogen bonding. The B3PW91 method makes use of Becke's three-parameter hybrid exchange functional[37] and the gradient correlated Perdew−Wang 1991 correlation functional.[38]

Nuclear Spin−Spin Coupling. Fermi contact (FC) contributions to the scalar coupling constants for the optimized structures were obtained at the unrestricted B3PW91/6-311G** triple-split level with polarization functions on hydrogen and heavier atoms. This approach combines DFT and finite perturbation theory (FPT) methods.[39] Calculated DFT/FPT results are based on the Fermi contact output of the FIELD option of Gaussian94.[40,41]

Of the four mechanisms generally considered to be important for nuclear spin−spin coupling,[42−45] only the Fermi contact (FC) components were computed here. Except for coupling constants involving fluorine, the FC contributions are often the most important. For example, recent computational studies included values for $^{1}J_{NH}$ and $^{h2}J_{NN'}$ for which the orbital diamagnetic and orbital paramagnetic contributions summed to −2.9 Hz and less than 0.1 Hz in magnitude,[21,22] respectively. Due to the greater difficulty of computing the spin−dipolar (SD) contributions to the scalar couplings, these contributions are often not reported. However, a recent ab initio study[23] of the formamide−formamidine dimer found that the SD contributions to $^{h1}J_{NH}$ and $^{h2}J_{NN'}$ were negligible. Although, these authors did not report a SD value for $^{1}J_{NH}$, a value of −0.23 Hz has been reported[46] for a planar arrangement of NH_3. The computed FC contribution (−87.2 Hz) in this arrangement is consistent with the calculated and experimental values in amides.

The combination of DFT and the finite perturbation theory method provides an excellent method for computing FC contributions to scalar coupling for low-*Z* elements. Unfortunately, the method provides no information about the associated electronic factors. It seems likely that the very great importance of scalar coupling in structural and conformational studies can be attributed to the early success of semiempirical [valence bond and molecular orbital (MO)] methods.[42,43] It is of interest here to see if a simple semiempirical MO treatment can assist with the interpretation of trans H-bonding coupling.

Analysis of Fermi Contact Coupling via a Simple LCAO-MO, Sum-over-States Model. In the delocalized MO model of Pople and Santry,[47,48] the FC contributions to the nuclear spin−spin coupling constant $J_{NN'}$ between nuclei N and N′ is given by

(25) Wijmenga, S. S.; Kruithof, M.; Hilbers, C. W. *J. Biomol. NMR* **1997**, *10*, 337−350.
(26) Schindler, M. *J. Am. Chem. Soc*. **1988**, *110*, 6623−6630.
(27) Facelli, J. C. *J. Biomol. Struct., Dyn.* **1998**, *16*, 619−629.
(28) Hu, J. Z.; Facelli, J. C.; Alderman, D. W.; Pugmire, R. J.; Grant, D. M. *J. Am. Chem. Soc*. **1998**, *120*, 9863−9869.
(29) Czernek, J.; Fiala, R.; Sklenar, V. *J. Magn. Reson.* **2000**, *145*, 142−146.
(30) Xu, X. P.; Au−Yeung, S. C. F. *J. Phys. Chem*. **2000**, *104*, 5641−5650.
(31) The Wüthrich convention[6] is used here: coupling constants over a single hydrogen bond are denoted ^{hx}J, where *x* is the number of bonds separating the coupled nuclei.
(32) Hobza, P.; Šponer, J. *Chem. Rev*. **1999**, *99*, 3247−3276 and references therein.
(33) Frisch, M. J.; Trucks, G. W.; Schlegel, H. B.; Gill, P. M. W.; Johnson, B. G.; Robb, M. A.; Cheeseman, J. R.; Keith, T.; Petersson, G. A.; Montgomery, J. A.; Raghavachari, K.; Al-Laham, M. A.; Zakrzewski, V. G.; Ortiz, J. V.; Foresman, J. B.; Cioslowski, J.; Stefanov, B. B.; Nanayakkara, A.; Challacombe, M.; Peng, C. Y.; Ayala, P. Y.; Chen, W.; Wong, M. W.; Andres, J. L.; Replogle, E. S.; Gomperts, R.; Martin, R. L.; Fox, D. J.; Binkley, J. S.; Defrees, D. J.; Baker, J.; Stewart, J. P.; Head-Gordon, M.; Gonzalez, C.; Pople, J. A. *Gaussian 94*, revision E.2; Gaussian, Inc.: Pittsburgh, PA, 1995.
(34) Hehre, W. J.; Radom, L.; Schleyer, P. v. R.; Pople, J. A. *Ab Initio Molecular Orbital Theory*; Wiley-Interscience: New York, 1986.
(35) Hohenberg, P.; Kohn, W. *Phys. Rev. B*. **1964**, *136*, 864−871. Kohn, W.; Sham L. J. *Phys. Rev. A* **1965**, *140*, 1133−1138.
(36) Parr, R. G.; Yang, W. *Density Functional Theory of Atoms and Molecules*; Oxford University Press: New York, 1989. March, N. H. *Electron Density Theory of Atoms and Molecules*; Academic Press: San Diego, CA, 1992.
(37) Becke, A. D. *J. Chem. Phys*. **1993**, *98*, 5648−5652.
(38) Wang, Y.; Perdew, J. P. *Phys. Rev. B* **1991**, *44*, 13298−13307. Perdew, J. P.; Wang, Y. *Phys. Rev. B.* **1992**, *45*, 13244−13249.
(39) Pople, J. A.; McIver, J. W., Jr.; Ostlund, N. S. *J. Chem. Phys*. **1968**, *49*, 2960−2964, 2965−2970.
(40) Onak, T.; Jaballas J.; Barfield, M. *J. Am. Chem. Soc*. **1999**, *121*, 2850−2856.
(41) Fierman, M.; Nelson, A.; Khan S. I.; Barfield, M.; O'Leary, D. J. *Org. Lett*. **2000**, *2*, 2077−2080.
(42) Barfield, M.; Grant, D. M. *Adv. Magn. Reson.* **1965**, *1*, 149−193.
(43) Barfield, M. In *Encyclopedia of NMR*; Grant, D. M., Harris, R. K., Eds., Wiley: New York, 1996; pp 2520−2532.
(44) Theoretical aspects of nuclear spin−spin coupling have been reviewed annually starting in 1972: Fukui, H. In *Nuclear Magnetic Resonance*; Specialist Periodical Reports 29; The Chemical Society London: London, 2000.
(45) Contreras, R. H.; Peralta, J. E.; Giribet, C. G.; de Azúa, M. C. R.; Facelli, J. C. *Ann. Rep. NMR Spectrosc.* **2000**, *41*, 57−166.
(46) de Azua, M. C. R.; Giribet, C. G.; Vizioli, C. V.; Contreras, R. H. *J. Mol. Struct. (THEOCHEM)* **1998**, *433*, 141−150.
(47) Pople, J. A.; Santry, D. P. *Mol. Phys*. **1964**, *7*, 269−286.
(48) Pople, J. A.; Santry, D. P. *Mol. Phys*. **1964**, *8*, 1−18.

$$J_{NN'} = \left(\frac{1}{4h}\right)\left(\frac{16\pi\beta\hbar}{3}\right)^2 \gamma_N\gamma_{N'} <t|\delta(r_N)|t><u|\delta(r_{N'})|u> \pi_{tu} \quad (1)$$

where t and u denote atomic or hybrid orbitals centered on nuclei N and N′, respectively, $\delta(r_N)$ and $\delta(r_{N'})$ are Dirac δ-functions evaluated at N and N′, respectively, and π_{tu} is the mutual atom−atom polarizability of Coulson and Longuet-Higgins,[49]

$$\pi_{tu} = 4\sum_{i,\mathrm{occ}}\sum_{j,\mathrm{unocc}}(\epsilon_i - \epsilon_j)^{-1} c_{it}c_{ju}c_{iu}c_{jt} \quad (2)$$

where c_{it} and c_{ju}, for example, denote the coefficients of orbital t and u in the ith and jth unoccupied MOs, respectively. The summations run over occupied and unoccupied MOs with energies ϵ_i and ϵ_j, respectively.

Magnetic Shielding Calculations. Magnetic shielding results were based on the gauge including atomic orbitals (GIAO) formulation[50,51] using DFT at the B3PW91/6-311G** level in Gaussian94.[33] The DFT functionals as implemented in the Gaussian94 codes do not include a specific magnetic field dependence.[52] All ^{1}H, and ^{15}N chemical shifts reported here are *isotropic* values which are indirectly referenced to tetramethylsilane (TMS) and liquid ammonia, respectively. Molecular structures for CH_4 and NH_3 were optimized at the B3PW91/6-31G** levels, and the ^{1}H and ^{15}N isotropic magnetic shieldings are 31.61 and 270.86 ppm, respectively, at the B3PW91/6-311G** level. The magnetic shielding of TMS was inferred from the experimental shift of gas-phase methane (0.13 ppm).[53,54] Similarly, the isotropic magnetic ^{15}N shielding (253.5 ppm) for the liquid ammonia reference makes use of the 399.3 ppm difference between gas-phase NH_3 and liquid CH_3NO_2[55,56] and the 381.9 ppm difference between liquid NH_3 and liquid CH_3NO_2.[57] Computations were performed using Silicon Graphics IRIS Origin 2000 and RISC 6000 IBM590 workstations.

Experimental Section

DFT simulations of Hoogsteen−Watson−Crick T·A−T and C$^+$·G−C base triplets were compared to NMR data obtained for a uniformly ^{13}C/^{15}N-labeled 32-nucleotide DNA oligonucleotide d(AGAGAGAACC CCTTCTCTCT TATATCTCTC TT) which forms the intramolecular DNA triplex with 8 base triplets depicted in Figure 1. The NMR sample preparation (1.5 mM DNA oligonucleotide, 100 mM NaCl, 5 mM $MgCl_2$, 95% H_2O/5% D_2O at pH 5.3) and the determination of $^{h1}J_{HN}$, $^1J_{HN}$, and $^{h2}J_{NN}$ coupling constants (as well as of the imino ^{1}H and ^{15}N chemical shifts) have been described previously.[3] Table 1 lists these parameters at 5 °C for the hydrogen-bonded N1−H1···N3, N3−H3···N1, and N3−H3···N7 atoms of the DNA triplex.

The sign determination of the $^{h2}J_{NN}$ coupling constant was carried out at 25 °C on a 600-MHz Bruker DMX spectrometer. The sample contained 1.6 mM uniformly ^{15}N/^{13}C-labeled potato spindle tuber viroid T1 RNA domain (69 nucleotides), 100 mM NaCl, 10 mM phosphate, 95% H_2O/5% D_2O, pH 6.0. The experimental scheme uses a simultaneous E.COSY-type detection of both $^{h1}J_{NH}$ and $^{h2}J_{NN'}$ couplings in U−A base pairs. The scheme consists of a two-dimensional, water flip-back ^{1}H−^{15}N TROSY[58] which detects the narrow ^{1}H3 and ^{15}N3 components of the uridine imino doublets. As a modification of this conventional TROSY, all ^{15}N pulses were applied as band-selective pulses which affect only the chemical shift region of the uridine ^{15}N3 donor nuclei (∼160 ppm). Therefore, the ^{15}N pulses do not disturb the spin states of the adenosine ^{15}N1 nuclei, which resonate around 230 ppm. During the t_1 and t_2 evolution periods, the uridine ^{15}N3 and ^{1}H3 spins evolve under the influence of the $^{h2}J_{NN'}$ and $^{h1}J_{NH}$ scalar couplings to the adenosine ^{15}N1 nucleus, respectively. Since this nucleus is in the same spin state during the entire experiment, an E.COSY-type pattern results.

Table 1. Chemical Shifts[a] and Coupling Constants[b] in the H−Bonding Regions of the DNA Triplex

	T25	C26	T27	C28	T29	C30	T31	T32
$\delta(^{15}N3)$	159.8	147.8	160.4	147.9	160.0	146.4	159.5	159.4
$\delta(^1H3)$	13.6	15.4	13.7	15.0	13.5	14.4	13.4	12.3
$^1J_{N3H3}$	−86.1	−85.9	−85.9	−84.2	−86.4	−86.1	−87.1	−88.7
$^{h2}J_{N3N7}$	7.1	10.4	7.8	10.9	8.2	10.3	8.1	6.6
$^{h1}J_{H3N7}$	nd[c]	nd	2.6	<2.1	2.7	<1.5	2.6	2.5
$\delta(^{15}N7)$	230.5	226.6	225.0	226.1	225.5	227.6	228.6	231.5
	A1	G2	A3[d]	G4[d]	A5[d]	G6[d]	A7	A8
$\delta(^{15}N1)$	221.5	145.7	221.2	145.2	221.2	145.2	222.3	221.7
$\delta(^1H1)$		12.6		12.6		12.6		
$^{1(h)}J_{N1H1}$	<2.1	−87.3	1.7	−87.8	1.7	−87.8	1.7	< 1.8
$^{h2}J_{N1N3}$	8.6	6.1	9.3	7.0	9.3	7.0	9.1	8.4
$^{1(h)}J_{N3H3}$	−85.3	2.8	−86.0	2.7	−86.0	2.7	−86.4	−85.5
$\delta(^1H3)$	14.7		14.2		14.2		14.2	14.8
$\delta(^{15}N3)$	160.2	194.9	160.6	194.7	160.6	194.7	160.9	161.3
	T20	C19	T18	C17	T16	C15	T14	T13

[a] All chemical shifts are in ppm. [b] All coupling constants are in hertz. $^{h1}J_{HN}$ and $^{h2}J_{NN}$ coupling constants are given as absolute values (see text). Values for $^1J_{HN}$ are assumed to have the same sign as the computed results for the FC terms. Estimated errors range from 0.1 to 0.3 Hz. [c] Not determined. [d] Due to a very similar chemical environment, the base pairs G$_4$·C$_{17}$, G$_6$·C$_{15}$ and T$_{16}$·A$_5$, T$_{18}$·A$_3$ have degenerate chemical shifts for both their diagonal and cross correlations. The *J*-coupling values correspond to averages of the degenerate base pairs.

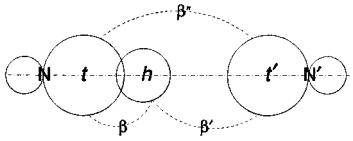

Figure 2. A simple model used to describe nuclear spin−spin coupling in the N−H···N′ hydrogen-bonding region. The hybrid orbital t centered on N is directed toward the 1s atomic orbital h on H, and t′ denotes a hybrid orbital on N′. The β's are resonance integrals associated with different pairs of orbitals.

Results and Discussion

Interresidue Coupling via a Sum-over-States Analysis of an N−H···N Fragment. Consider the N−H···N moiety depicted in Figure 2. This consists of sp^2 hybrid orbitals t and t′ on N and N′, respectively, and the 1s atomic orbital h on hydrogen. Molecular orbitals are given as a linear combination of a 1s atomic orbitals h on hydrogen and hybrid-type orbitals t and t′ on nitrogen.

$$\chi = c_1\mathrm{t} + c_2\mathrm{h} + c_3\mathrm{t}' \quad (3)$$

With the usual approximations including the neglect of the resonance integral β'' in Figure 2, MO energies and wave functions can be obtained analytically from the 3 × 3 secular

(49) Coulson, C. A.; Longuet-Higgins, H. C. *Proc. R. Soc. London, Ser A* **1947**, *191*, 39−60. Coulson, C. A.; Longuet-Higgins, H. C. *Proc. R. Soc. London, Ser A* **1948**, *193*, 447−464.

(50) For general reviews of theory of magnetic shielding, see, for example: Jameson, C. J.; De Dios, A. C. In *Nuclear Magnetic Resonance;* Specialist Periodical Reports 29; The Chemical Society London: London, 2000; and previous chapters in this series.

(51) Ditchfield, R. *Mol. Phys.* **1974**, *27*, 789−807

(52) Becke, A. D. *Can. J. Chem.* **1996**, *74*, 995−997.

(53) Emsley, J. W.; Feeney, J.; Sutcliffe, L. H. *High-Resolution Nuclear Magnetic Resonance*; Pergamon: New York, 1966; Vol. 2. The experimental gas-phase data were converted as described by Kutzelnigg et al.[54]

(54) Kutzelnigg, W.; Fleischer, U.; Schindler, M. In *NMR Basic Principles and Progress*; Diehl, P., Fluck, E., Kosfeld, R., Eds.; Springer: Berlin, 1990; Vol. 23, pp 165−262.

(55) Mason, J. In *Multinuclear NMR*; Mason, J., Ed.; Plenum: New York, 1987; pp 335−367.

(56) Litchman, W. M.; Alei, M., Jr.; Florin, A. E. *J. Chem. Phys.* **1969**, *50*, 1031−1032. Alei, M., Jr.; Florin, A. E.; Litchman, W. M.; O'Brien, J. F. *J. Phys. Chem.* **1971**, *75*, 932−938.

(57) Witanowski, M.; Stefaniak, L.; Webb, G. A. *Ann. Rep. NMR Spectrosc.* **1993**, *25*, 88.

(58) Pervushin, K.; Riek, R.; Wider, G.; Wüthrich, K. *Proc. Natl. Acad. Sci U.S.A.* **1997**, *94*, 12366−12371

determinant. From eq 2, the mutual atom−atom polarizabilities for the three types of trans hydrogen-bonding couplings include only two terms in the summations

$$\pi_{tt'} = -\frac{\gamma^2}{2\beta(1+\gamma^2)r^{3/2}}\left(\frac{12r+a^2}{4r-a^2}\right) \quad (4)$$

$$\pi_{th} = -(1/2\beta r^{3/2}) \quad (5)$$

$$\pi_{ht'} = -(\gamma^2/2\beta r^{3/2}) \quad (6)$$

where

$$r = 1+\gamma^2+\frac{a^2}{4}, \quad \gamma = \beta'/\beta, \quad a = (\alpha_h - \alpha_t)/\beta \quad (7)$$

where β and β' are the resonance integrals as labeled in Figure 2 and α_h and α_t denote Coulomb integrals. Since β is inherently negative, all three mutual atom−atom polarizabilities have positive signs. Since ^{15}N and ^{1}H in eq 1 have magnetogyric ratios of opposite sign, $^{h2}J_{NN'}$ is predicted to have a positive sign, while $^{1}J_{NH}$ and $^{h1}J_{HN}$ are both predicted to be negative.

According to the approximate methods of Mulliken[59] and Laforgue,[60] a in eqs 4−7 is empirically related to the difference in electronegativities of hydrogen and nitrogen.

$$a = E_N - E_H \quad (8)$$

The Pauling electronegativities for nitrogen and hydrogen are 3.0 and 2.1,[61] respectively, and thus lead to a value $a = 0.9$. All three coupling constants are predicted to decrease in magnitude as the electronegativity differences increase.

In semiempirical theories of *J*-coupling, the integrals over the Dirac δ-functions in eq 1 lead to s-orbital densities s^2(N) and s^2(N′) which are treated as parameters. The values used by Pople et al.[39] are s^2(N) = 6.9265 au and s^2(H) = 0.372 au, respectively. Resonance integrals β and β' in the above equations were taken to be proportional to overlap integrals, e.g., $\beta = -10$ eV S. Assuming the nominal values of 1.04 and 1.80 Å for r_{NH} and $r_{H\cdot\cdot N}$ in the N−H···N′ fragment of Figure 2, one can make some crude estimates of the values of the coupling constants. Overlap integrals evaluated over Slater-type orbitals using the formulas of Mulliken et al.[62] for hybrid orbitals lead to $\beta = 6.3$ eV and $\beta' = 2.6$ eV. Substituting these values into eqs 1 and 4−7 gives the following: $^{h2}J_{NN'} = 31$ Hz, $^{1}J_{NH} = -86$ Hz, and $^{h1}J_{HN} = -15$ Hz. The second of these is in fortuitously good agreement with the experimental data, but $^{h2}J_{NN'}$ and $^{h1}J_{HN}$ have substantially larger magnitudes than the values reported here. Moreover, the experimental data[2] and the DFT/FPT results suggest positive signs for both $^{h2}J_{NN'}$ and $^{h1}J_{HN}$ at typical base pair H···N′ distances. It seems likely that these disparities are attributable, in part, to the neglect of the interactions between the hydrogen and the other orbitals on N′. In Figure 3, the three trans H-bonding coupling constants, which are based on eq 1 and eqs 4−7, are plotted as a function of γ in the range 0−1. If r_{NH} is fixed at 1.04 Å, then this range of γ correponds to decreasing $r_{H\cdot\cdot N}$ from a value > 3.5 Å to 1.04 Å. The behavior of the three curves follows from the expressions for the mutual atom−atom polarizabilities. These equations show how the three types of spin−spin coupling depend on the *electronic* part of eq 1. The numerator of π_{th} is unity in eq 5, while $\pi_{tt'}$ and $\pi_{ht'}$ in eqs 4 and 6 are proportional to γ^2. Therefore, as γ approaches zero, the directly bonded coupling has its maximum absolute value and the trans H-bonding coupling constants vanish. The directly bonded coupling constant $^{1}J_{NH}$ decreases in magnitude as the hydrogen approaches N′ and becomes equal to $^{h1}J_{NH}$ for $\gamma = 1$ corresponding to the hydrogen at the midpoint of the hydrogen bond. In the limit $a^2 \ll 1$ and $\gamma^2 \ll 1$, the mutual atom−atom polarizability $\pi_{tt'}$ (eq 4) is 3 times $\pi_{ht'}$ (eq 6). This implies that the electronic features associated with the "two-bond" coupling should be 3 times that for the "one-bond" interresidue coupling. Additionally in eq 1, the nitrogen s-electron density is almost 19 times larger than for hydrogen [s^2(N)/s^2(H) = 18.7]. This more than compensates for the smaller ^{15}N magnetogyric ratio ($\gamma_N/\gamma_H = -0.10$) and is a factor in the larger magnitudes observed for $^{h2}J_{NN}$ coupling constants. This is consistent with the DFT and experimental mangnitudes described in the next section, but the negative sign for $^{h1}J_{NH}$ *over the entire range* of the parameter γ is an error of this simple model.

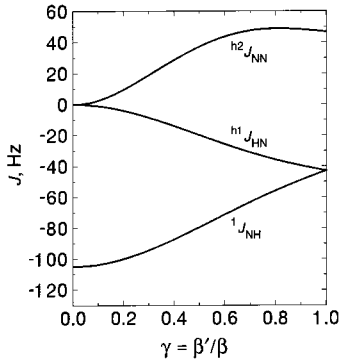

Figure 3. Semiempirical MO results for nuclear spin−spin coupling constants $^{h2}J_{NN'}$, $^{h1}J_{NH}$, and $^{1}J_{NH}$ in N−H···N′ plotted as a function of $\gamma = \beta'/\beta$. Coupling constants at $\gamma = 0$ correspond to $r_{NH} = 1.04$ Å, $r_{HN'} \geq 3.5$ Å and at $\gamma = 1$, $r_{NH} = r_{HN'} = 1.04$ Å.

Determination of the Sign of $^{h2}J_{NN'}$. The DFT results presented here and in the previous study[3] are in agreement with the positive sign of the $^{h1}J_{HN}$ in Watson−Crick DNA base pairs. Both DFT simulations and the three-orbital model (Figure 3) of the N−H···N system predict that $^{h2}J_{NN}$ is also positive. However, experimental evidence for the latter has not been previously presented. Figure 4 shows an experimental determination of the sign of $^{h2}J_{NN}$. This was carried out on the ^{13}C/^{15}N-labeled, left-terminal RNA domain of the potato spindle tuber viroid.[1] Clearly visible in Figure 4 are such E.COSY-type splittings of the uridine ^{15}N3−^{1}H3 correlations. A quantification of the splittings yields values of approximately 7 ($^{h2}J_{NN'}$) and 2−3 Hz ($^{h1}J_{NH}$), respectively. The negative slope of the E.COSY pattern indicates that $^{h2}J_{NN'}$ and $^{h1}J_{NH}$ have the same sign since the magnetic moments of ^{1}H and ^{15}N are of opposite signs. As the $^{h1}J_{NH}$ couplings have been determined to be positive,[2] this indicates that the $^{h2}J_{NN'}$ coupling is also positive in accordance with theoretical predictions.[3,21−23]

DFT Geometries of the Bases, Dimers, and Triplets. Geometries for the two triplets depicted in Figure 1, and the five model nucleotides (1-methylcytosine, its cation, 9-methylguanosine, 1-methylthymine, and 9-methyladenine) were fully optimized at the B3PW91/6-31G** level. Methyl groups replace ribose groups in the model *trimers* used to represent the C$^+$·G−C and T·A−T triplets depicted in Figure 1. Table 2 lists the computed structural and NMR data in the imino H-bonding

(59) Mulliken, R. S. *J. Chim. Phys.* **1949**, *46*, 497−542.
(60) Laforgue, A. *J. Chim. Phys.* **1949**, *46*, 568−592.
(61) Pauling, L. *The Nature of the Chemical Bond*, 3rd ed.; Cornell University Press: Ithaca, NY, 1960; p 89.
(62) Mulliken, R. S.; Rieke, C. A.; Orloff, D.; Orloff, H. *J. Chem. Phys.* **1949**, *17*, 1248−1267.

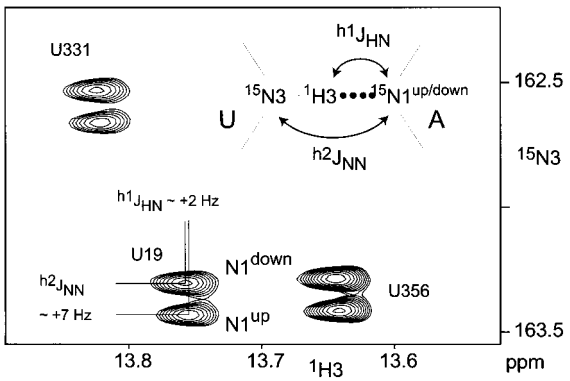

Figure 4. Determination of the sign of the $^{h2}J_{NN'}$ coupling by E.COSY−TROSY observation of the $^{h2}J_{NN'}$ and $^{h1}J_{NH}$ couplings in the U−A base pairs of the left terminal domain of the potato spindle tuber viroid.[1] The $^{1}H-^{15}N$ TROSY spectrum was recorded with excitation of the ^{15}N resonances restricted to the uridine $^{15}N3$ region by means of selective sinc pulses (300 ms for 90°) centered at 163 ppm. The data matrix consisted of 150($t1$) × 1024($t2$) data points with acquisition times of 150 ($t1$) and 71 ms ($t2$). Total experimental time was 18 h.

regions. Results for each trimer are given for the respective dimeric subunits: C$^+$·G and G−C in C$^+$·G−C, T·A and A−T in T·A−T.

Results for the model dimers used to model the G−C and A−U base pairs (appropriate to RNA), which were described previously, are included in Table 2 for comparison.[1] For each of these dimers, two sets of optimizations were performed. In one set only, the hydrogen atom positions were optimized with heavy atom positions from a 1.16-Å crystal structure.[63] In the other calculations, all atom positions were optimized. It is striking how well the fully optimized structures of the G−C and A−U dimers reproduce the geometry of experimentally determined high-resolution structures. For example, the N1···N3 distances r_{NN} of the fully optimized structures are 2.914 (C−G) and 2.823 Å (U−A) whereas a survey of all the base pairs in the 1.16-Å resolution structure of the acceptor stem of tRNA^{Ala} (NDB entry AR0009)[63] gives values of 2.91 ± 0.08 Å (N = 8) for C−G and of 2.83 ± 0.06 Å (N = 4) for A−U base pairs. The crystal structure exhibits ring nonplanarity (7.6° and 4.5° for C−G and A−U, respectively) as measured by the ∠C2−C4−C6−C2 angles, which are less than 0.1° for the fully optimized structures.

The optimized structures (B3PW91/6-31G**) for both dimers and trimers retain the planar arrangement of the bases relative to each other and reproduce the expected hydrogen bond pattern. This is in contrast to a recent molecular dynamics simulation[64] of A−T and G−C base pairs using the empirical AMBER force field. In that study, Watson−Crick pairing and the relative planarity of the base pairs could not be obtained without the introduction of additional, empirical constraints. These results indicate, therefore, that a full quantum-mechanical treatment of the base pairs, i.e., of electrons, nuclei, and their interactions, is sufficient to reproduce their complete geometry including the hydrogen bond pattern without the necessity for any further restraints. In particular, the forces resulting from the attachment of the base to the nucleic acid backbone are not necessary to hold the base pairs "in place".

The entries in Table 2 are listed in order of increasing separation r_{NN} between the donor and acceptor nitrogen atoms. The shortest separation (2.662 Å) occurs for the charged $N_3\cdots N_7$ hydrogen bond of the C$^+$·G−C trimer. Inter-nitrogen separations for the other four hydrogen-bonded species fall within a relatively narrow range of 2.86 ± 0.05 Å. Also included in the table are the covalent bond lengths of the donor group r_{NH}. Since the latter have exponential dependencies on r_{NN},[65] the shorter r_{NN} value for the C$^+$·G dimeric unit leads to a substantially elongated N−H bond. From the computed internal angles ∠N−H···H, it can be seen that the largest deviation from linearity is 7°. Also entered in Table 2 are relevant structural and NMR data for the five model monomer bases. All covalent N−H bond lengths for the monomers are substantially shortened as expected in the absence of hydrogen bonding.

The Dependence of Computed NMR Parameters on r_{NN} in the Model Trimers. Included in Table 2 are the FC contributions to the coupling constants $^{h1}J_{NH}$, $^{h2}J_{NN'}$, and $^{1}J_{NH}$ in the trans hydrogen-bonding regions of the nucleic acid trimers, dimers, and monomers. Also included are the computed ^{1}H chemical shifts $\delta(^{1}H)$ and the ^{15}N chemical shifts of the acceptor $\delta(N_a)$ and donor $\delta(N_d)$ nitrogen atoms. Several NMR parameters, e.g., $^{h2}J_{NN'}$ and $\delta(^{1}H)$, suggest a dependence on r_{NN} but others, especially the ^{15}N chemical shifts, vary considerably for different residues. The results presented in the following sections elaborate these points and show in detail how the various NMR parameters in the H-bonding region depend on the interresidue dimer separations.

Starting with the optimized trimer geometries, coupling constants and chemical shifts were obtained for C$^+$·G−C and T·A−T trimers by varying the distances between the base pairs.[66] For example, the data plotted in Figures 5 and 6 (filled circles and solid lines) apply to the C$^+$·G hydrogen-bonding region of the C$^+$·G−C triplet depicted in Figure 1. These plots demonstrate how the NMR parameters are predicted to vary as the methylcytosine cation C$^+$ is translated relative to G−C. Using results in the C$^+$·G dimer region of the C$^+$·G−C trimer as an example, the following computational strategies were used to investigate the dependencies of the NMR parameters on r_{NN} and r_{NH}:

(1) All NMR calculations started with the C$^+$·G−C trimer structure, which was fully optimized at the B3PW91/6-31G** level.

(2) The trimer was rotated so that the x-axis was along the N3−N7 line.

(3) All atoms of the 1-methylcytosine cation C$^+$ were translated along the x-axis such that the N3···N7 distance was 2.6 Å.

(4) The position of the imino hydrogen H3 was optimized (B3PW91/6-31G**) while the positions of all other trimer atoms were constrained. A value of 1.099 Å was obtained for r_{NH} and the ∠N3−H3···N7 angle was 175.4° for r_{NN} = 2.6 Å. The C$^+$ atoms were shifted by an additional 0.1 Å along the x-axis, and the computational procedure was repeated to provide NMR data as a function of r_{NN} in the range 2.6−4.0 Å. The N3−H3 bond lengths exhibit the expected exponential decrease as r_{NN} increases.

In another set of calculations, the N1−N3 distances between C$^+$·G and the methylcytosine atom were shifted over the same range while the geometry of C$^+$·G−C and C was held at the optimized values. Similarly, calculations were performed whereby the T·A and A−T distances of the T·A−T trimers were varied.

(63) Mueller, U.; Schubel, H.; Sprinzl, M.; Heinemann, U. *RNA* **1999**, *5*, 5670−677.
(64) Stofer, E.; Chipot, C.; Lavery, R. *J. Am. Chem. Soc.* **1999**, *121*, 9503−9508.
(65) Steiner, T. *Chem. Commun.* **1995**, 1331−1332.
(66) The dependencies of NMR data and the optimized r_{NH} on r_{NN} are tabulated in the Supporting Information.

Table 2. Calculated Structural and NMR Data in the Trans H-Bonding Regions of Species That Model RNA and DNA Base Pairs, Triplets, and Nucleotides[a]

base pair	aggr	dnr	acp	r_{NN} (Å)	r_{NH} (Å)	∠N−H·N (deg)	$^1J_{NH}$ (Hz)	$^{h2}J_{NN}$ (Hz)	$^{h1}J_{NH}$ (Hz)	$\delta(^1H)$ (ppm)	$\delta(N_a)$ (ppm)	$\delta(N_d)$ (ppm)
C^+·G	trimer	C^+−N3	G−N7	2.662	1.098	175.6	−67.7	12.8	−1.8	19.5	236.9	168.8
T·A	trimer	T−N3	A−N7	2.806	1.048	175.6	−76.8	7.4	3.5	15.0	248.8	175.8
G−C[b]	dimer	G−N1	C−N3	2.817	1.040	173.0	−78.8	6.7	3.4	14.6	203.8	158.5
U−A	dimer	U−N3	A−N1	2.823	1.053	179.6	−75.9	7.5	2.7	15.4	231.8	177.9
T−A	trimer	T−N3	A−N1	2.825	1.053	180.0	−76.1	7.4	2.7	15.4	234.4	175.6
U−A[c]	dimer	U−N3	A−N1	2.843	1.050	177.0	−79.7	7.1	2.6	15.1	229.4	178.4
G−C	trimer	G−N1	C−N3	2.903	1.045	180.0	−77.7	6.2	2.8	14.3	210.0	157.4
G−C	dimer	G−N1	C−N3	2.914	1.036	178.2	−77.1	5.4	3.3	13.2	211.1	157.7
C^+[·G][d]	monomer	C^+−N3	G−N7		1.015		−82.5			7.1	280.7	150.3
G[-C][d]	monomer	G−N1	C−N3		1.013		−75.8			6.3	233.0	156.4
T[-A][d]	monomer	T−N3	A−N1		1.012		−79.0			6.6	252.5	166.3
A[·T][d]	monomer	T−N3	A−N7		1.012		−79.0			6.6	259.7	166.3
U[-A][d]	monomer	U−N3	A−N1		1.011		−78.8			6.5	252.5	167.3

[a] In all cases, computed results apply to model compounds in which the ribose functions are replaced by methyl groups. Unless noted otherwise, structures are fully optimized at the B3PW91/6-31G** level. Coupling constants are based on the DFT/FPT method at the UB3PW91/6-311G**//B3PW91/6-31G** level; chemical shifts are obtained from the DFT/GIAO procedure at the B3PW91/6-311G**//B3PW91/6-31G** level. The ^1H and ^{15}N chemical shifts are indirectly referenced to TMS and liquid ammonia based on the values obtained at the same levels (31.61 and 270.86 ppm for CH_4 and NH_3, respectively. The experimental values for CH_4 is $\delta = 0.13$ ppm. The liquid NH_3 reference made use of the 399.3 ppm difference between gas NH_3 and liquid CH_3NO_2 and the 381.9 ppm difference between liquid NH_3 and liquid CH_3NO_2. [b] Structural data for the heavy atoms according to the second G−C base pair of NDB entry AR0009,[63] with optimized hydrogen positions. [c] Structural data for the heavy atoms according to the U−A base pair of NDB entry AR0009,[63] with optimized hydrogen positions. [d] Monomer data are listed for the imino group of the donor as well as for the chemical shift of the acceptor nitrogen atom (listed in brackets) where both donor and acceptor nucleotides were calculated as monomers.

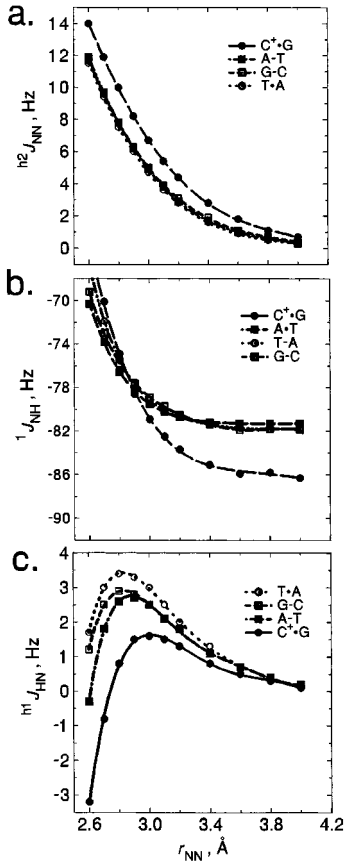

Figure 5. DFT/FPT Fermi contact contributions to trans H-bonding coupling constants plotted versus interresidue separations $r_{NN'}$: (a) $^{h2}J_{NN'}$, (b) $^1J_{NH}$, and (c) $^{h1}J_{NH}$. Data for C^+·G, A−T, T·A, and G−C are represented by filled circles (solid line), filled squares (dot−dash line), open circles (dotted line), and open squares (short-dashed line), respectively. For the continuous lines, the computed data were interpolated by third- to fifth-order polynomial fits.

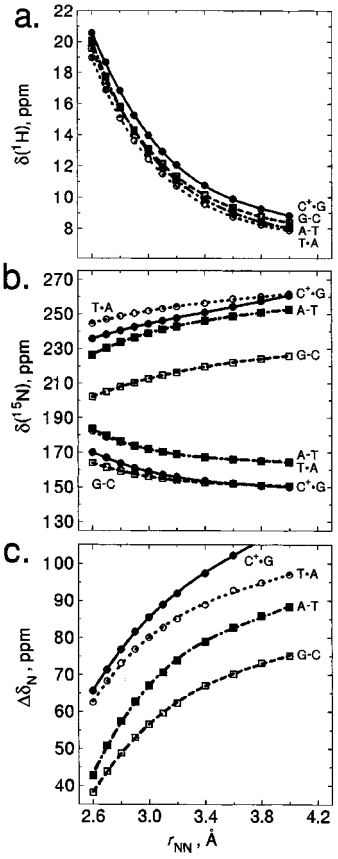

Figure 6. DFT/GIAO isotropic ^1H and ^{15}N chemical shifts in the trans H-bonding region plotted versus interresidue separations $r_{NN'}$: (a) $\delta(^1H)$, (b) $\delta(N_a)$ for acceptor nitrogens in the range 200−260 ppm and $\delta(N_d)$ for donor nitrogens in the range 150−180 ppm, and (c) $\Delta\delta_N = \delta(N_a) - \delta(N_d)$.

The only difference in the procedure for T·A−T was in step 4 wherein the positions of the imino hydrogens were optimized in the T·A and A−T dimers rather than the trimers. Since the values were very close to those in the trimer, this substantially reduced the computational time.

Plotted in Figures 5 and 6 are the results of these calculations for the four base pair types C^+·G, G−C, T·A, and A−T of the DNA triplets. In general, the calculated parameters exhibit very

similar dependencies on the donor−acceptor distance for all base pair types. As expected, variation of r_{NN} in the range 2.6−4.0 Å gives only a single energy minimum (energy data are not shown) which coincides in all four cases to the fully optimized geometry.

The interresidue dependencies of the computed coupling constants $^{h2}J_{NN'}$, $^{1}J_{NH}$, and $^{h1}J_{NH}$ and chemical shifts $\delta(^{1}H)$, $\delta(^{15}N_a)$, and $\delta(^{15}N_d)$ on r_{NN} are depicted in Figures 5a−c and 6a,b, respectively.[66] With the exception of $^{h1}J_{NH}$, all the NMR parameters depend monotonically on the interresidue separation; that is, $^{h2}J_{NN'}$, $^{1}J_{NH}$, $\delta(^{1}H)$, and $\delta(^{15}N_d)$ decrease whereas $\delta(^{15}N_a)$ increases with increasing donor−acceptor distance. In contrast, the $^{h1}J_{NH}$ scalar coupling (Figure 5c) shows a more irregular behavior exhibiting distinct positive maximums near 2.8 Å for T·A, G−C, and A−T and near 3.0 Å for C^+·G base pairs. Negative values of $^{h1}J_{NH}$ are predicted for C^+·G donor−acceptor distances less than ∼2.8 Å. The prediction of positive $^{h1}J_{NH}$ for normal Watson−Crick donor−acceptor distances greater than this value is consistent with the experimental observations of Pervushin et al.[2] in an ^{15}N-labeled 14-mer DNA duplex.

As would be expected for decreasing hydrogen bond interactions, the trans H-bond coupling constants $^{h2}J_{NN'}$ and $^{h1}J_{NH}$ (Figure 5a and c, respectively) approach zero as the bases are separated. For large separations, the $^{1}J_{NH}$ (Figure 5b) coupling constant asymptotically approaches −80 to −86 Hz corresponding to the directly bonded ^{1}H−^{15}N coupling constants of the free bases. Clearly, the magnitudes of the latter are underestimated by 10−20% as compared to experimentally observed values of approximately −90 Hz. Similar underestimates of other types of $^{1}J_{XH}$ couplings[40] have been attributed to the neglect of vibrational motions.

The three coupling constants (Figure 5) and the imino proton chemical shifts (Figure 6a) for the G−C, T·A, and A−T base pairs exhibit very similar dependencies on $r_{NN.}$ The data for the C^+·G base pair are predicted to follow the same trends but deviate in magnitude from the other base pairs. These data show that the chemical differences of G−C, T·A, and A−T base pairs do not strongly affect either $^{h2}J_{NN'}$, $^{1}J_{NH}$, $^{h1}J_{NH}$, or $\delta(^{1}H)$.

The different behavior of the C^+·G base pair must be linked to the net positive charge of its donor group and the influence of long-range ion−dipole interactions. This longer range behavior of the C^+·G base pair is indeed observed for $^{h2}J_{NN'}$, $^{1}J_{NH}$, $\delta(^{15}N_a)$, and $\delta(^{15}N_d)$. A flattening of the dependence on r_{NN} occurs only for substantially larger distances when compared to the other base pairs in Figures 5a, 5b, and 6b.

At first sight, the decrease of $^{h1}J_{NH}$ to negative values for small donor−acceptor distances seems rather confusing. However, this behavior as well as the trends for the $^{1}J_{NH}$ coupling and the donor and acceptor chemical shifts, $\delta(^{15}N_d)$ and $\delta(^{15}N_a)$, can be understood from simple symmetry considerations which are implicit in Figures 2 and 3. Decreasing the donor−acceptor distance r_{NN} with a fixed covalent bond length r_{NH} centers the proton between the nitrogen atoms. In this symmetric arrangement[20] the $^{h1}J_{NH}$ would be approximately equal to $^{1}J_{NH}$. From Figure 3, values of about −40 Hz would be expected. However, the different electronic environments of donor and acceptor atoms in their respective ring systems break this symmetry to some extent. For example, a DFT/FPT calculation for the proton arranged symmetrically in the T·A dimer (r_{NN} = 2.6 Å) of T·A−T leads to the computed FC values $^{h2}J_{NN'}$ = 16.0 Hz, $^{1}J_{NH}$ = −35.4 Hz, and $^{h1}J_{NH}$ = −24.7 Hz. Since DFT/FPT values for the normal, asymmetric H-bonds are typically positive (Figure 5c), moving the hydrogen to the midpoint of the H-bond implies a change in sign for $^{h1}J_{NH}$. A similar symmetrization of the donor and acceptor ^{15}N chemical shifts is observed in Figure 6b, where $\delta(^{15}N_d)$ increases while $\delta(^{15}N_a)$ decreases with decreasing base separation. Thus, the trends of both one-bond coupling constants and of the donor and acceptor chemical shifts seem to follow from simple symmetry considerations.

The chemical shift $\delta(^{1}H)$ of the imino proton (Figure 6a) is strongly influenced by the base separation and depends in a very similar manner on r_{NN} as the trans H-bond coupling $^{h2}J_{NN'}$. Such a behavior has been noted previously in the simulation of a 16-atom G−C base pair fragment.[3] These theoretical findings corroborate experimental observations of strong correlations between the chemical shift of the hydrogen-bonded proton and the value of the trans H-bond couplings $^{h2}J_{NN}$ and $^{h3}J_{NC}$, in nucleic acids[3] and proteins,[5] respectively.

Coupling constants and proton chemical shifts for the different base pairs (with the possible exception of C^+·G) exhibit very similar dependencies on base pair separations. By way of contrast, the calculated ^{15}N chemical shifts (Figure 6b) differ substantially at a given N−N distance depending on the type of base pair. This is expected because different chemical environments in the aromatic ring systems strongly influence ^{15}N chemical shifts. Additional evidence for this influence is found in Hoogsteen T·A and Watson-Crick T-A base pairs where the donor groups are identical, but the acceptor groups are different: there, very similar ^{15}N chemical shifts are obtained for the donor thymine N3 nitrogens (Figure 6b). In contrast, the influence of the acceptor group (A−N3 or A−N1) on the chemical shift of the donor ^{15}N nucleus seems negligible.

In general, the choice of a reference for computed chemical shifts is difficult. In the case of ^{15}N chemical shifts this problem is aggravated by the fact that the usual calculated reference is *gas-phase* NH_3 and the experimental results for biopolymers are indirectly referenced to *liquid* NH_3. Differences $\Delta\delta_N = \delta(^{15}N_a) - \delta(^{15}N_d)$ in the ^{15}N chemical shifts of the acceptor and donor nitrogen atoms cancel to some extent this ambiguity in the referencing, the neglect of solvent effects, and interactions from other parts of the DNA molecule. Figure 6c shows the dependence of the differences $\Delta\delta_N$ on the donor−acceptor distance r_{NN}. Since the chemical shifts of donor and acceptor nitrogens decrease and increase, respectively, with increasing base separation, their difference $\Delta\delta_N$ covers a larger range than either $\delta(^{15}N_a)$ or $\delta(^{15}N_d)$ alone.

Comparisons of Calculated and Experimental Results. To perform a meaningful comparison of the calculated and observed NMR parameters with structural factors such as the internuclear separations, knowledge of the molecular coordinates with a precision better than ∼0.1 Å would be a prerequisite. This precision is not currently available for the structure of the DNA triplex, which was determined by conventional NMR techniques.[67] As an alternative, it is possible to examine the adequacy of the calculated and experimental interdependencies. For example, the very good linear correlation between $^{h2}J_{NN'}$ and $\delta(^{1}H)$ was noted previously.[3] Figure 7a shows plots of both the calculated and the experimental $^{h2}J_{NN'}$ versus $\delta(^{1}H)$. The dashed line passing through the experimental points is that obtained in the linear regression of the experimental data,

$$^{h2}J_{NN'} = 1.32\delta(^{1}H) - 10.1 \text{ Hz}, \quad r^2 = 0.756 \qquad (9)$$

The computed values for the four base pairs exhibit very good linear correlations between $^{h2}J_{NN'}$ and $\delta(^{1}H)$($r^2 \geq 0.999$) over

(67) Tarköy, M.; Phipps, A. K.; Schultze, P.; Feigon, J. *Biochem.* **1998**, *37*, 5810−5819.

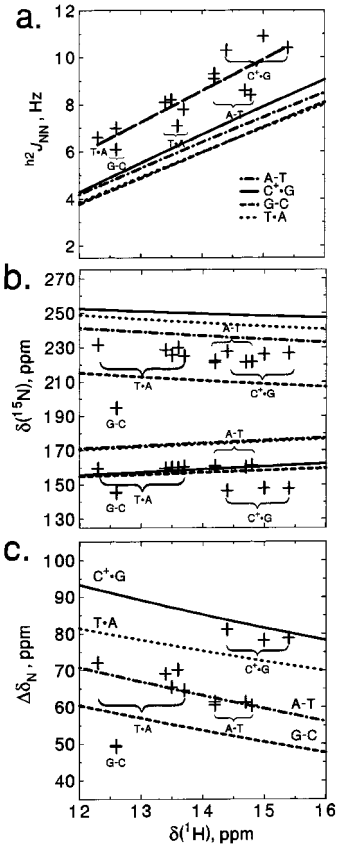

Figure 7. Plots of (a) DFT/FPT coupling constants $^{h2}J_{NN'}$ versus the DFT/GIAO isotropic chemical shifts $\delta(^1H)$, (b) DFT/GIAO isotropic ^{15}N chemical shifts δ_N [$\delta(N_a)$ and $\delta(N_d)$ for acceptor and donor, respectively] versus ^1H chemical shifts $\delta(^1H)$, and (c) difference $\Delta\delta_N$ in the ^{15}N chemical shifts for acceptor and donor, plotted versus ^1H chemical shifts $\delta(^1H)$. For all plots, the corresponding experimental data are plotted versus one another (plus signs). In (a), the line with the long dashes follows from the linear regression.

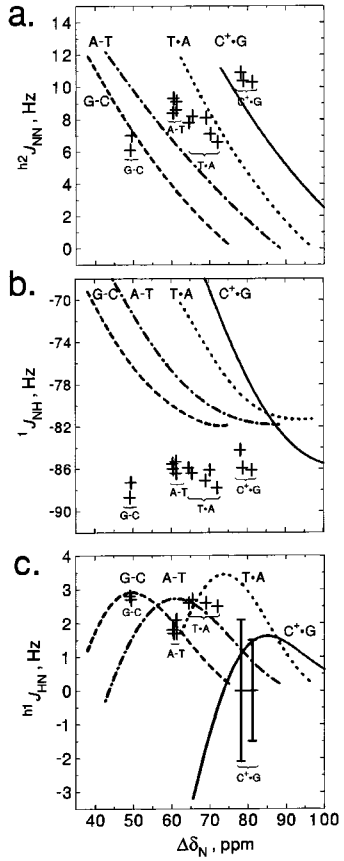

Figure 8. Plots of (a) coupling constants $^{h2}J_{NN'}$ versus the ^{15}N isotropic chemical shifts $\Delta\delta_N$, (b) coupling constants $^1J_{NH}$ versus the ^{15}N chemical shifts $\Delta\delta_N$, and (c) coupling constants $^{h1}J_{HN}$ versus the ^{15}N chemical shifts $\Delta\delta_N$. In all plots, the corresponding experimental data are plotted versus one another (plus signs). Error bars are given for C^+·G.

the whole range (2.6−4.0 Å). The slopes and intercepts range from 0.98 (A−T) to 1.15 (C^+·G) Hz·ppm^{-1} and −7.8 (A−T) to −9.4 (C^+·G) Hz, respectively. The disparities between the calculated results and the experimental data in the figures are reasonable considering that the calculations were performed for the isolated trimers. They do not reflect electronic environments produced by the complex intra- and intermolecular interactions from solvent and other parts of the DNA triplex. For example, the stacking of base pairs would lead to nonnegligible ring current effects. The calculated and experimental ^{15}N chemical shifts for the donor $\delta(N_d)$ and acceptor nitrogens $\delta(N_a)$ are plotted in Figure 7b as a function of the $\delta(^1H)$. Since $\delta(^1H)$ decreases with r_{NN}, the slopes for $\delta(N_a)$ and $\delta(N_b)$ in Figure 7b are opposite to those in Figure 6b. Clearly, the DFT/GIAO results overestimate the experimental chemical shifts by 15−20 ppm. However, the slopes of the calculated data are in reasonable agreement with the experimental data. Therefore, the comparisons with experimental data are somewhat better depicted via plots of the differences $\Delta\delta_N$ versus $\delta(^1H)$ in Figure 7c. The plot of $\Delta\delta_N$ versus $\delta(^1H)$ in Figure 7c shows correspondence between calculated and experimental $\Delta\delta_N$ for C^+·G and A−T but overestimates the data for the other two base pairs by ∼10 ppm.

Since the $\Delta\delta_N$ exhibit the greatest variations for a given internuclear distance, plots of the NMR parameters versus $\Delta\delta_N$ more effectively spread out the calculated results and experimental data along the horizontal axis. For each dimer type, these provide a better indication of the dependence of NMR parameters on r_{NN}. There are probably too few experimental data points in this study to detect any significant patterns, but the data for the T·A and A−T pairs exhibit trends that are consistent with the calculated ones. It should be possible to infer information about interresidue dependencies of the NMR parameter for individual base pairs.

Plots of the calculated and experimental data for the three types of coupling constants versus $\Delta\delta_N$ are given in Figure 8. Figure 8a includes plots of the calculated and experimental $^{h2}J_{NN'}$ versus $\Delta\delta_N$. In all of the panels, the experimental data cluster according to base pair type. Variations of the parameter within the clusters presumably reflect different interresidue separations. This is most obvious in the data for the T·A dimer, which exhibits the largest variations. The magnitudes of all directly bonded $^{15}N-^1H$ coupling constants $^1J_{NH}$ are underestimated by ∼10 Hz (Figure 8b). It seems likely that noncontact mechanisms contribute only ∼30% of this disparity.[21−23] All computed coupling constants apply to gas-phase molecules at fixed internuclear distances. The experimental data reflect rovibrational averaging, medium effects, and interbase interactions. The importance of these various factors is not known for this type of directly bonded coupling. In the case of CH_4, it has been shown[68] that the magnitude of the directly bonded $^{13}C-^1H$ coupling constant computed at the equilibrium distance should be ∼4% less than the 125-Hz experimental gas-phase value. It is also known that gas-to-solution shifts of directly bonded coupling constants can be substantial for polar molecules in solvents of high dielectric constant.[69]

The trans H-bond coupling constants $^{h1}J_{NH}$ are plotted versus $\Delta\delta_N$ in Figure 8c. Even though this type of coupling exhibits the most complicated dependence on structural factors, the experimental points fall reasonably close to the computed curves for each of the four bases. The $^{h1}J_{NH}$ for the C$^+$·G dimer were too small to be measured. The error bars are upper limits for the absolute values.

From the values of the experimental NMR parameters and the computed results for the trimers at the optimized geometries, it appears that interresidue N−N distances range from about 2.7 to 3.1 Å. On the basis of the plots of NMR parameters, it seems likely that $^{h2}J_{NN'}$, $\delta(^1H)$, and $\Delta\delta_N$ will prove to be valuable for investigating structural features in the H-bonding region. Depending on base pairs, the slopes for $^{h2}J_{NN'}$ range from −14.2 to −18.3 Hz·Å^{-1}, $\delta(^1H)$ covers a range around −13.4 to −16.6 ppm·Å^{-1}, and $\Delta\delta_N$ ranges from 36 to 50 ppm·Å^{-1}. Based on these numbers and the experimental results for the various triplets, three independent estimates are obtained for the ranges over which the r_{NN} vary along the triple helix. The averages and standard deviations of the variations in the interresidue distances for C$^+$·G, T·A, A−T, and G−C are 0.05 ± 0.01, 0.13 ± 0.06, 0.04 ± 0.01, and 0.02 ± 0.02 Å, respectively. These ranges are consistent with data for the tRNA^{Ala} crystal structure. Furthermore, the largest changes in the experimental NMR parameters occur for the T32·A8 base pair. Since this base pair terminates the DNA chain in Figure 1, it is expected to exhibit the greatest effects of fraying. The numbers given above suggest that the interresidue distance r_{NN} for the T32·A8 base pair would be increased by 0.1−0.2 Å in comparison with T·A base pairs in the interior of the triplex.

Conclusions

Density functional methods were used to calculate the Fermi contact contributions to nuclear spin−spin coupling constants and the isotropic chemical shifts in H-bonding regions of C$^+$·G−C and T·A−T Hoogsteen−Watson−Crick triplets. Computations were also performed as a function of interresidue separation for the four types of base pairs. Each type of NMR parameter is strongly and similarly dependent on r_{NN}. They are also strongly interrelated, in conformity with the experimental results. Inter-relationships among the imino proton isotropic chemical shifts, ^{15}N isotropic chemical shifts, and $^1J_{NH}$ have been recognized for some time. This work provides a theoretical framework for their interpretation.

The NMR parameters for T·A, A−T, and G−C base pairs exhibit very similar dependencies on r_{NN}. The variations of the experimental data points should be indicative of base pair separations. Considering the spectral complexity and size of these molecules, the results are quite reasonable and could be used to predict coupling constants in these molecules. An independent electron model is used for a qualitative investigation of coupling constants around the hydrogen bond. According to this model $^{h2}J_{NN}$ and $^{h1}J_{HN}$ should both increase in magnitude with increasing hydrogen bond strength, while $^1J_{NH}$ is predicted to decrease.

Acknowledgment. We thank James Masse for synthesizing the DNA triplex sample. Appreciation is extended to Udo Heinemann and Uwe Müller for making the tRNA^{Ala} crystal structure available to us prior to publication. A.J.D. is a recipient of an Australian National Health and Medical Research Council C. J. Martin Fellowship (Regkey 987074). This work was funded by SNF grant 31-61′757.00 to S.G. and NIH grants GM37254 and GM48123 to J.F.

Supporting Information Available: (1) Structures of optimized dimers and trimers (Cartesian coordinates or *z*-matrix formats), (2) for each dimer pair in the trimers, a table (Table 3) of computed coupling constants, chemical shifts, and r_{NH} plotted versus inter-nitrogen separations r_{NN}, and (3) a table of data (Table 4) in which the computed data from Table 3 were fit to an exponential form $a_0 + (a_1 + a_2 \cdot r_{NN}^2)\exp[-b(r_{NN} - r_{eq})]$. (print/PDF). This material is available free of charge via the Internet at http://pubs.acs.org.

JA003781C

(68) Wigglesworth, R. D.; Raynes, W. T.; Sauer, S. P. A.; Oddershede, J. *Mol. Phys.* **1997**, *92*, 77−88 and references therein.
(69) Barfield, M.; Johnston, M. D., Jr. *Chem. Rev.* **1973**, *73*, 53−73.